Solution-processed graphene films for electrochemical monitoring of extracellular nitric oxide released by breast cancer cells

2D Materials

PAPER

Solution-processed graphene films for electrochemical monitoring of extracellular nitric oxide released by breast cancer cells

Derrick Butler[1,2,5,6], **Chinmay S Sankhe**[3,5], **Pouya Soltan Khamsi**[1], **Esther W Gomez**[3,4] and **Aida Ebrahimi**[1,2,4,*]

[1] Department of Electrical Engineering, Pennsylvania State University, University Park, PA 16802, United States of America
[2] Center for Atomically Thin Multifunctional Coatings, Pennsylvania State University, University Park, PA 16802, United States of America
[3] Department of Chemical Engineering, Pennsylvania State University, University Park, PA 16802, United States of America
[4] Department of Biomedical Engineering, Pennsylvania State University, University Park, PA 16802, United States of America
[5] Equal contribution.
[6] Current address: National Institute of Standards and Technology, Gaithersburg, MD 20899, United States of America
* Author to whom any correspondence should be addressed.

E-mail: sue66@psu.edu

Keywords: nitric oxide, electrochemical, sensor, graphene, L-arginine, fibronectin

Supplementary material for this article is available online

OPEN ACCESS

RECEIVED
29 June 2023

REVISED
31 October 2023

ACCEPTED FOR PUBLICATION
5 December 2023

PUBLISHED
20 December 2023

Abstract

Nitric oxide (NO) plays an important role in cardiovascular function, immune response, and intercellular signaling. However, due to its short lifetime, real-time detection of NO is challenging. Herein, an electrochemical sensor based on fibronectin-modified, solution-processed graphene ink for NO detection is developed using a facile fabrication method involving spin-coating and hot-plate annealing. The sensor is first electrochemically characterized with a NO donor, spermine NONOate, exhibiting a dynamic range of 10–1000 μM. The fibronectin-functionalized graphene supports the attachment and growth of MDA-MB-231 breast cancer cells, as confirmed by optical microscopy. Extracellular NO production is stimulated using the amino acid L-arginine. NO production results in morphological changes to the adhered cells, which are reversible upon the addition of the NO synthase antagonist Nω-nitro-L-arginine methyl ester. The production of NO is also confirmed using real-time amperometric measurements with the fibronectin-functionalized graphene sensors. While this work focuses on NO detection, this potentially scalable platform could be extended to other cell types with envisioned applications including the high-throughput evaluation of therapeutics and biocompatible coatings.

1. Introduction

Nitric oxide (NO) is an important small molecule produced from amino acid L-arginine by the nitric oxide synthase (NOS) enzyme family (Michel and Feron 1997). NO is involved in numerous physiological functions, including vasodilation as an endothelium-derived relaxation factor, immune system function, and neurological processes in the brain (Heales *et al* 1999, Habib and Ali 2011, Maiorana *et al* 2012, Džoljić *et al* 2015). Moreover, NO plays an important role in both promoting and inhibiting tumor growth, depending upon the concentration, timing, and location (Xu *et al* 2002, Korde Choudhari *et al* 2013). Relatively high levels of NO, particularly associated with macrophages (Macmicking *et al* 1997), can have tumoricidal effects (Garbán and Bonavida 1999). On the other hand, NO can cause oxidative damage to DNA (Derojas-Walker *et al* 1995), which could lead to deleterious mutations and tumor promotion (Korde Choudhari *et al* 2013). Furthermore, NOS expression has been reported in various cancer cell types, including breast cancer (Reveneau *et al* 1999, Vakkala *et al* 2000, Loibl *et al* 2002). For MDA-MB-231 triple negative breast cancer cells, NO induces the upregulation of NOS and cancer biomarkers, alters cell migration, and impacts the response of the MDA-MB-231 cells to chemotherapeutic agents (Heinecke *et al* 2014). Additionally, NOS expression in breast cancer cells

promotes metastasis and has been correlated to poor prognosis and poor patient outcomes (Walsh *et al* 2016, Chung *et al* 2021). Given the importance of NO in health and life science, and especially its role in cancer, monitoring and quantifying NO concentration and dynamics is important for understanding disease progression and for the development of novel therapeutics.

Numerous methods have been reported for the detection of NO, including fluorescence measurement (Lim *et al* 2006), colorimetric assays (Sun *et al* 2003), electron paramagnetic resonance spectroscopy (Weaver *et al* 2005), and chemiluminescence measurement (Pinder *et al* 2008). Fluorescent probes, for example, are being used for *in vitro* and *in vivo* applications due to their high sensitivity and their ability to be used for spatial monitoring of NO, especially in biological media (Lim *et al* 2006). Although effective, many of these methods are endpoint measurements, which are not conducive to detecting NO in real-time. In contrast, electrochemical sensors have the potential to enable monitoring NO levels in real-time, especially if they are interfaced closely with the source of NO (Guo *et al* 2022). The ability to monitor changes in NO level continuously compared to periodically (e.g. cyclic voltammetry (CV)) can be advantageous given the short lifetime of NO and its rapid dynamics. Recent examples of electrochemical sensors for NO detection are based on noble metals (e.g. Au, Pt, Ag) and their nanostructures (Zhang and Oyama 2005, Quinton *et al* 2011, Thi Kim *et al* 2014, Govindhan and Chen 2016), two-dimensional (2D) materials (e.g. graphene, transition-metal dichalcogenides, MXenes) (Liu *et al* 2013, 2015, Yoon *et al* 2017), transition metal compounds/nanostructures (Shahid *et al* 2015, Wang *et al* 2021) and protein-functionalized electrodes (Wu *et al* 2010, Chen and Zhao 2012). The 2D materials are especially interesting for electrochemical applications due to the large surface-to-volume ratio and in some cases, high electrical conductivity and biocompatibility (Bolotsky *et al* 2019, Nguyen *et al* 2020, Rohaizad *et al* 2021). In particular, graphene, a 2D allotrope of carbon, has shown remarkable properties (such as high conductivity and biocompatibility) and as a result, has seen widespread use in electrochemical sensing (Suvarnaphaet and Pechprasarn 2017). Numerous reports have shown graphene modified with gold (Ting *et al* 2013, Li *et al* 2015, Geetha Bai *et al* 2017), platinum (Mathew *et al* 2021), or bimetallic nanoparticles (Govindhan and Chen 2016, Liu *et al* 2016). In an effort to move away from noble metal usage, other examples have demonstrated graphene-based NO sensors modified with peptides (Guo *et al* 2012), for example. Even sensors for NO based on graphene with varying degrees of oxidation have been reported (Liu *et al* 2013), although no measurement of extracellular NO has been reported in this particular example. Another report shows remarkably low detection limits and high sensitivities with hemin-functionalized graphene, along with the capability for real-time extracellular NO detection (Jiang *et al* 2013). Despite the exceptional performance, the mechanical exfoliation technique used to prepare the graphene limits the scalability of this technology. Alternatively, the ability to prepare graphene directly in solution has enabled its production on an increasingly larger scale, which is crucial for enabling future high-throughput and low-cost applications.

Herein, we explore solution-processed graphene ink for real-time electrochemical detection of extracellular NO secreted by human breast cancer cells that are grown directly on the graphene surface. The graphene films are prepared on silicon substrates using a simple two-step spin-coating and annealing process. By functionalizing the graphene surface with the extracellular matrix protein fibronectin, cells can attach and proliferate directly on the graphene film, which is in good agreement with previous reports (Kenry *et al* 2016). Close contact between the graphene and cell layer is crucial because of the short lifetime (one to tens of seconds, Conner and Grisham 1995, Thomas *et al* 2001, Habib and Ali 2011) of NO. The generation of extracellular NO is confirmed electrochemically using chronoamperometry measurements with L-arginine as an NOS protagonist. The generation of NO can be halted by the addition of Nω-nitro-L-arginine methyl ester (L-NAME), a NOS antagonist. Furthermore, optical microscopy is utilized to visually inspect the effect of NO production on cell morphology, which changes drastically after the addition of L-arginine and then reverts upon addition of L-NAME. While this work demonstrates the detection of NO generation, the biocompatibility and electrochemical properties of the solution-processed graphene films make the developed sensing chips a well-suited platform to investigate other systems, such as neurotransmitter release from neural cells and drug screening.

2. Materials and methods

2.1. Materials and reagents

The graphene ink is purchased from Millipore-Sigma. The Spermine NONOate (SN) is purchased from Cayman Chemical and stored at −80 °C until use. Dulbecco's phosphate buffered saline (PBS, pH 7.4) and Dulbecco's Modified Eagle's Medium (DMEM) are purchased from Corning Inc. L-arginine, L-NAME, (3-mercaptopropyl) trimethoxysilane (MPTS), and toluene (anhydrous) are purchased from Sigma-Aldrich. Fibronectin is purchased from Gibco. Fetal bovine serum (FBS) is purchased from Atlanta Biologicals and gentamicin is purchased from Gibco. Si/SiO_2 wafers are purchased from NOVA Wafers (285 nm, wet thermal oxide,

p-type). Acetone and isopropanol (IPA) are purchased from VWR. Polydimethylsiloxane (PDMS, Sylgard 184) is prepared in a 10:1 ratio of elastomer to curing agent, degassed under vacuum, and cured at ∼60 °C in an oven.

2.2. Preparation of graphene ink films

The graphene films are prepared using a similar strategy as reported previously (Butler *et al* 2021). The 1 × 1 cm^2 Si/SiO_2 chips are ultrasonicated sequentially in acetone and IPA for 15 min each followed by rinsing in deionized water (Milli-Q, 18.2 MΩ cm) and drying under N_2 flow. The chips are then immersed overnight in MPTS (5% by vol. in toluene) at room temperature. Then, the chips are rinsed with toluene and dried. The 60 μl of graphene ink is spin-coated on each chip at 5000 rpm for 30 s. After spin-coating, the samples are annealed on a hot plate at 300 °C for 30 min under ambient conditions.

2.3. Device assembly

The spin-coated and processed graphene films are contacted using copper tape. To passivate the copper tape and ensure a consistent active sensor area, a piece of polyimide tape with a 4 mm diameter hole punched out is attached to the Si/SiO_2 chip. For measurements with cells, a PDMS well (8 mm diameter) is attached to the sensor using a thin layer of Ecoflex (Smooth-On Inc.) and cured at room temperature for at least 1 h.

2.4. Material characterization

Scanning electron microscopy images are acquired in a ThermoFisher Verios instrument at a working distance of 2.6 mm. The graphene films are not coated with any conductive layer for imaging and are grounded to the sample chuck using copper tape. X-ray photoelectron spectroscopy (XPS) measurements are carried out using a Physical Electronics VersaProbe II instrument (Chanhassen, MN). An Al Kα x-ray source is used at 45° takeoff angle. Charge neutralization is carried out using low energy (<5 eV) electrons and Ar ions. Raman measurements are performed with a Horiba LabRAM instrument using a 532 nm laser and 300 gr mm^{-1} grating. The spectra are measured in 10 × 10 s acquisitions. Spectra of three distinct areas are measured and the mean and standard deviation values are calculated.

2.5. Electrochemical characterization

Electrochemical measurements are performed with either a PalmSens4 single-channel or MultiPalmSens4 multi-channel potentiostat. Ag/AgCl (3 M NaCl) is used as the reference electrode and Pt wire is used as the counter electrode. CV measurements are performed at a scan rate of 50 mV s^{-1} unless otherwise specified. Electrochemical impedance spectroscopy (EIS) measurements are performed at a DC potential of 0 V vs. the open-circuit potential and a small AC signal of 5 mV. Chronoamperometry measurements with SN in N_2-purged PBS are performed in a C3 Cell Stand (Bioanalytical Systems Inc.) at a potential of 0.8 V vs. Ag/AgCl and a magnetic stirrer at 400 rpm. N_2 blankets the solution during the measurement. The current is allowed time to reach an approximately steady-state before adding SN. The SN solutions are held in a 37 °C water bath when not in use.

2.6. Cell culture

The human breast cancer cell line MDA-MB-231 (HTB-26), purchased from the American Type Culture Collection (ATCC), is used for this study and the cells are grown according to the recommendations of ATCC. MDA-MB-231 cells are maintained in DMEM supplemented with 10% FBS and 50 μg ml^{-1} gentamicin. Media is changed every 3 d, and the cells are grown in a 37 °C incubator in a humidified 5% CO_2 environment.

2.7. Fibronectin coating

The PDMS wells mounted on graphene ink are sterilized with 70% ethanol for 5 min and are washed with 1× PBS twice. Fibronectin solution in 1× PBS is pipetted onto the wells and incubated for 2 h at room temperature. Fibronectin concentrations of 10, 25, and 50 μg ml^{-1} are used to examine cell attachment to the graphene ink substrate. A fibronectin concentration of 25 μg ml^{-1} is used for coating the graphene for electrochemical assays and is kept constant for all the samples across different measurements. Fibronectin concentration was used as recommended by the manufacturer and is consistent with literature studies that have used fibronectin for cell adherence of MDA-MB-231 breast cancer cells (Maity *et al* 2011, Taherian *et al* 2011, Frahs *et al* 2019).

2.8. Seeding cells onto the graphene film

The graphene ink samples coated with fibronectin are washed with 1× PBS twice to remove excess fibronectin and 200 μl of cell culture growth medium is added into the wells. MDA-MB-231 cells are seeded at a density of 10 000 cells per well (50 000 cells ml^{-1}). The devices are then placed in the incubator at 37 °C to allow for the cells to attach to the fibronectin-coated graphene surface.

2.9. Treatments with L-arginine and L-NAME

For electrochemical assays, 72 h post-seeding, cells are taken out of the incubator, and media is aspirated from the wells. The cells are washed with 1× PBS twice before adding fresh 1× PBS. The counter and reference electrodes are inserted into each well and connections are made to the potentiostat. Stock concentrations of 50 mg ml^{-1} of L-arginine and L-NAME are made in water. After achieving the baseline

reading, cells are treated with 4 mM L-arginine or a combination of 4 mM L-arginine and 8 mM L-NAME. The control samples without the cells containing only 1× PBS are also treated with the same concentrations. The electrochemical assay is then performed for 1 h.

2.10. Morphological assays

For morphological studies, cells are seeded on fibronectin-coated glass substrates and fibronectin-coated graphene ink-coated glass substrates. The 24- or 72 h post-seeding, cells are taken out of the incubator, and media is aspirated. The cells are washed with 1× PBS twice before adding fresh 1× PBS. Cells are then treated with 4 mM L-arginine or a combination of 4 mM L-arginine and 8 mM L-NAME and incubated for 2 h. Cells are imaged with a 20× objective on a Nikon Eclipse Ti-E inverted fluorescence microscope equipped with a Photometrics CoolSNAP HQ2 camera. Imaging conditions and settings were kept constant for all sample treatments. Cell spread area and cell aspect ratio are determined from phase contrast images using the 'shape descriptors' measurement tool in ImageJ software. Data are reported for at least 170 cells for each experimental condition. An analysis of variance followed by Tukey's post hoc test was performed using Minitab software for sample comparison. Differences between the means of the cell spread area and the aspect ratio for various treatment conditions were considered significant for p-values less than 0.05.

2.11. Live/dead assay

Assessment of cell viability following treatments with L-arginine and the combination of L-arginine and L-NAME was performed using a ThermoFisher LIVE/DEAD viability/cytotoxicity kit as per the manufacturer's recommended protocol. Briefly, following treatment of cells with the stimulants for 2 h, the cells were washed with 1× PBS and treated with 2 μM of calcein AM and 4 μM ethidium homodimer-1 for 30 min at room temperature. The treated samples were then visualized using fluorescence microscopy. Cells are imaged with a 10× or 20× objective on a Nikon Eclipse Ti-E inverted fluorescence microscope equipped with a Photometrics CoolSNAP HQ2 camera.

3. Results and discussion

3.1. Preparation and characterization of fibronectin-modified graphene ink films

Preparation of the graphene films begins by spin-coating a commercially available graphene ink onto a SiO_2/Si wafer. The samples are then annealed at 300 °C for 30 min on a hot-plate to remove any remaining solvent and decompose the stabilizing polymer in the ink, hence improving the electrical conductivity (Secor *et al* 2015). The resulting graphene film is comprised of individual graphene flakes approximately 100–400 nm in lateral size as determined by atomic force microscopy (figure 1(a)). Raman spectroscopy (figure 1(b)) confirms the presence of the characteristic Raman bands for graphitic carbon species. A comparison of the D peak intensity, which is attributable to defects present in the graphene lattice, to the G peak can provide an estimate of the defect density in the graphene film (Ferrari and Robertson 2004, Cançado *et al* 2011). A ratio (I_D/I_G) of 0.39 ± 0.01 is indicative of a moderate defect density, noting that some amount of defects can be advantageous for electrochemical applications due to significantly faster electron transfer at defect sites (Zhong *et al* 2014).

In addition to Raman spectroscopy, XPS measurements are performed to elucidate the elemental composition of the samples. Figure 1(c) shows a representative survey spectrum with carbon, oxygen, and silicon peaks present with atomic percentages of 89.3 ± 1.3, 8.1 ± 0.8, and 2.6 ± 0.5 ($n = 3$), respectively. While carbon and oxygen are to be expected for graphene, the presence of silicon is attributed to the underlying substrate. Figure 1(d) provides a high-resolution spectrum of the C 1s region. The main sp^2 carbon feature at ∼284.4 eV is fitted using an asymmetric peak (Kovtun *et al* 2019) with a line shape determined by measuring freshly cleaved highly-ordered pyrolytic graphite (pure sp^2 carbon). The tail of the asymmetric peak has been shown to provide a better quantification of the oxygen functional groups present on the graphene surface (Kovtun *et al* 2019). After fitting the sp^2 feature, smaller symmetric peaks corresponding to sp^3 defects and various oxygen functional groups are fitted: sp^3 (285.0 eV), C–OH (285.6 eV), C–O–C (286.8 eV), C=O (288.0 eV), and O–C=O (289.0 eV). Lastly, two broad peaks at binding energies 6.4 and 10.1 eV higher than the main sp^2 feature are attributed to plasmon/shake-up contributions (Leiro *et al* 2003, Kovtun *et al* 2019).

In order to promote cell attachment, the graphene film is functionalized with fibronectin (Quinton *et al* 2011), which is an extracellular matrix protein. Electrochemical characterization before and after the fibronectin treatment is undertaken to confirm the successful functionalization of the graphene film (figure 2) without completely hindering its electrochemical activity. CV with 5 mM $[Fe(CN)_6]^{4-}$ shows the characteristic oxidation and reduction peaks for exemplary samples with and without fibronectin (figure 2(a)). After fibronectin modification, the electron transfer is more sluggish, as indicated by the suppression and increased separation of the redox peaks, with ΔE_{peak} increasing from 209.5 ± 39.3 mV to 346.8 ± 23.8 mV ($n = 4$). Moreover, the peak ratio (I_{ox}/I_{red}) increases from 1.07 ± 0.07 to 1.66 ± 0.31, noting an ideal value of 1. EIS measurements are also carried out to complement the CV analysis. EIS

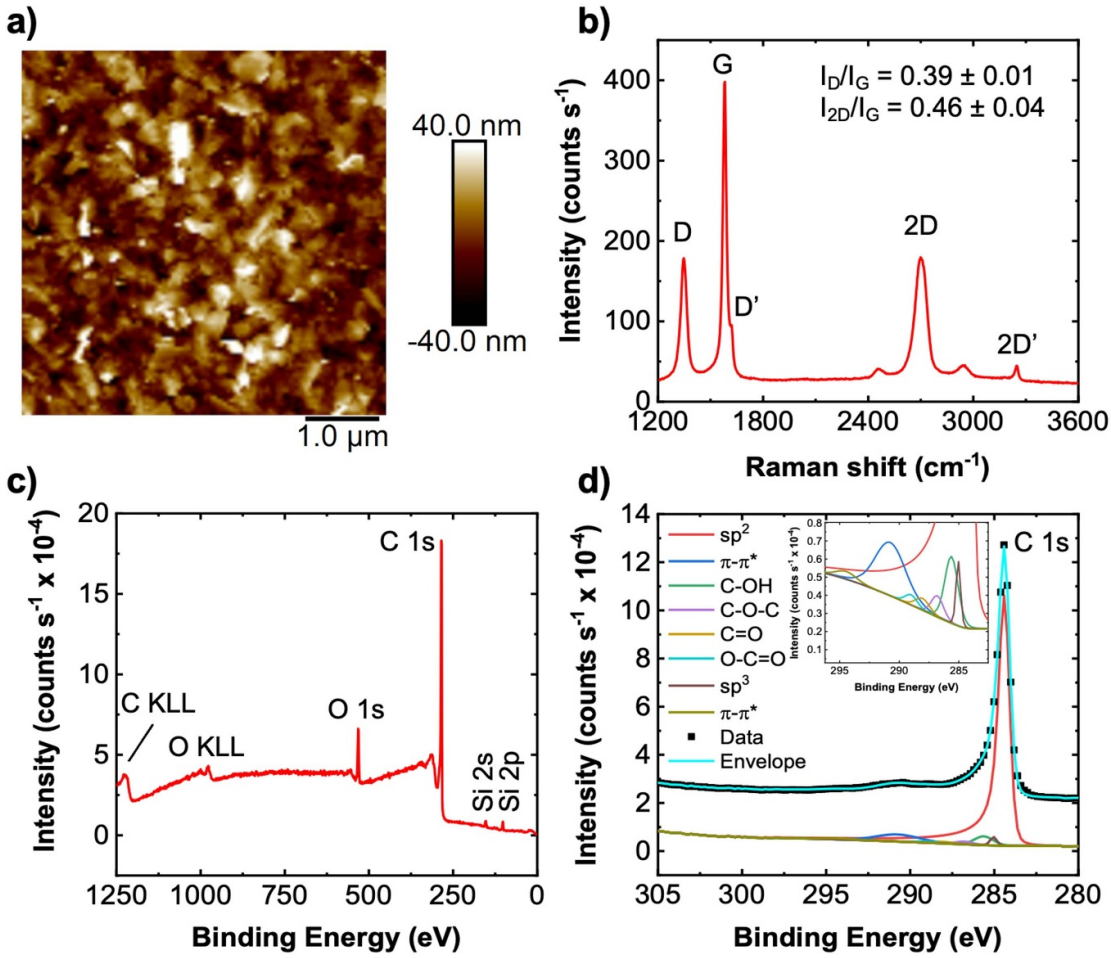

Figure 1. Material characterization of graphene films. (a) An exemplary atomic force micrograph of the spin-coated graphene film. (b) Raman spectrum of the graphene film ($\lambda = 532$ nm). Peak ratios are determined from spectra recorded at 3 distinct locations on the same sample. (c) An x-ray photoelectron spectroscopy (XPS) survey scan demonstrating the elemental composition of the graphene film. (d) A high-resolution XPS scan of the carbon 1s region and corresponding peak fitting of the various components.

probes the interfacial charge transfer at the electrode surface by applying a small (5 mV) AC signal of varying frequency centered at the open circuit potential (Bard *et al* 2022). The exemplary Nyquist plots shown in figure 2(c) are modeled using a modified Randles circuit (SI figure S1), whereby the double-layer capacitance term (C_{dl}) is replaced by a constant phase element (Q_{CPE}) to account for heterogeneities at the electrode surface (Córdoba-Torres *et al* 2015). The solution resistance (R_s) is consistent for samples with and without fibronectin modification (figure 2(d)), which is expected as the electrolyte is the same. The charge transfer resistance (R_{ct}), an indication of the facility of the redox reaction, is found to increase from 9.19 ± 4.31 kΩ to 36.99 ± 10.86 kΩ after fibronectin treatment, which is consistent with the CV data. Surface modification with a protein layer commonly leads to an increased charge transfer resistance as the proteins effectively slow or 'block' the electron transfer (Tolba *et al* 2012). Overall, the more sluggish electron transfer kinetics seen after fibronectin modification allude to the successful functionalization of the graphene, which is important for efficient cell attachment and growth on the electrode surface.

3.2. Electrochemical characterization with synthetic NO

After preparing the graphene films, the electrochemical response is benchmarked with synthetic NO. To do so, we employ a NO donor, SN, to prepare serial aliquots of NO in a N_2-purged PBS solution. SN is chosen due to its previously characterized decomposition kinetics (Ramamurthi and Lewis 1997), where the authors reported a maximum NO concentration that was approximately ten-fold less than the initial SN concentration and occurred after ∼10 min. This timeframe corresponds well to experimental timeframes, whereas other NONOates, such as diethylamine NONOate and diethylenetriamine NONOate, have very rapid or lengthy decomposition kinetics, respectively. First, we perform CV measurements at a scan rate of 50 mV s^{-1} with a range of SN concentrations to characterize the oxidation of NO

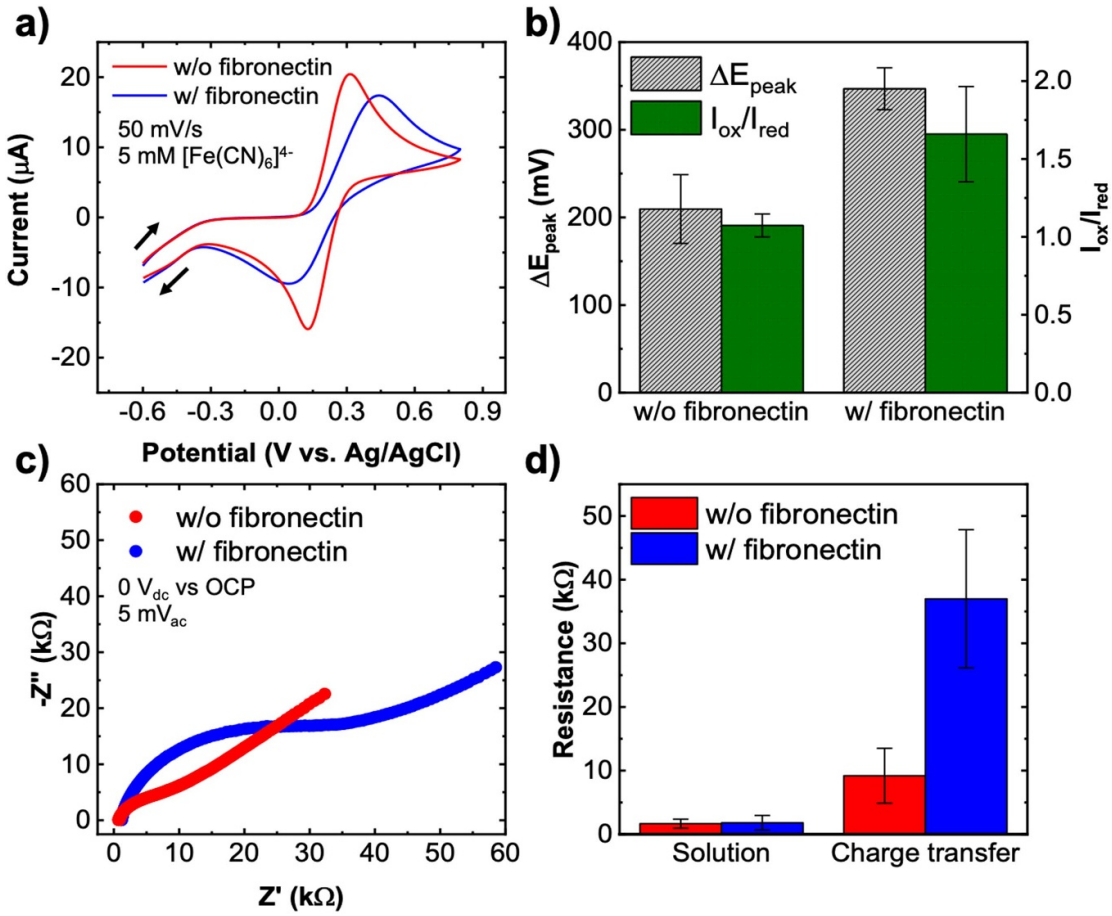

Figure 2. Modification of the graphene film with fibronectin. (a) Cyclic voltammograms from −0.6 V to 0.8 V with 5 mM $[Fe(CN)_6]^{4-}$ in PBS before and after fibronectin treatment (scan rate = 50 mV s^{-1}). (b) The resulting peak separation (ΔE_{peak}) and peak ratio (I_{ox}/I_{red}) as determined from CV measurements ($n = 4$). (c) Electrochemical impedance spectroscopy measurements before and after fibronectin modification (V_{dc} = open circuit potential, $V_{ac} = 5$ mV). (d) The extracted charge transfer and solution resistance from EIS measurements ($n = 4$).

(figure 3(a)). From the CV data, a concentration-dependent oxidation wave can be seen at ∼0.9 V vs. Ag/AgCl, which is in agreement with previous reports of electrochemical NO sensors (Shahid *et al* 2015, Liu *et al* 2016). The resulting calibration curve, $\frac{\Delta I}{I_0} = \frac{I-I_0}{I_0} \times 100$ where I is the current at a particular SN concentration and I_0 is the baseline current in the absence of SN, measured at 0.96 V vs. Ag/AgCl is shown in figure 3(b). For the region from 10 to 1000 μM SN, the fitting equation (equation (1), $R^2 = 0.9998$) is,

$$\log_{10}\left(\Delta I/_{I_0}(\%)\right) = 0.748 \times \log_{10}([\mathrm{SN}]\ (\mu\mathrm{M})) + 1.281 \quad (1)$$

In addition to CV measurements, chronoamperometry at a constant potential of 0.8 V vs. Ag/AgCl is performed to characterize the sensor response in real time. Figure 3(c) shows the current-time data after a 10 min stabilization period for SN concentrations from 67 nm to 36 μM. The lower panel of figure 3(c) provides a closer look at early time points where small undulations in current can be seen for SN concentrations as low as 0.13 μM. Well-defined steps in current can be seen at a SN concentration of 0.73 μM, noting the actual NO concentration will be lower (Ramamurthi and Lewis 1997, Majumder *et al* 2014). To determine the response time of the graphene sensor, we focus on the well-defined step after adding 6.4 μM of SN. Based on these results, we estimate a response time at 95% of the resulting current to be 17.7 s. While the response time is not as short as other reports (Xu *et al* 2014), perhaps due to the reduced electron transfer rate caused by the presence of fibronectin, the amperometric measurements indicate that the sensor responds reasonably well in real-time at nM-level concentrations of NO. Previous reports have implicated *in vitro* and *in vivo* levels of NO to be in the range of pM to μM depending on the cell type, tissue type, expression of NOS isoforms, experimental design, and measurement approach (Nagano 1999, He and Liu 2001, Mocellin *et al* 2007, Hall and Garthwaite 2009, Liu *et al* 2017, Dou *et al* 2019). A comparison of this work to related graphene-based NO sensors is provided in table 1.

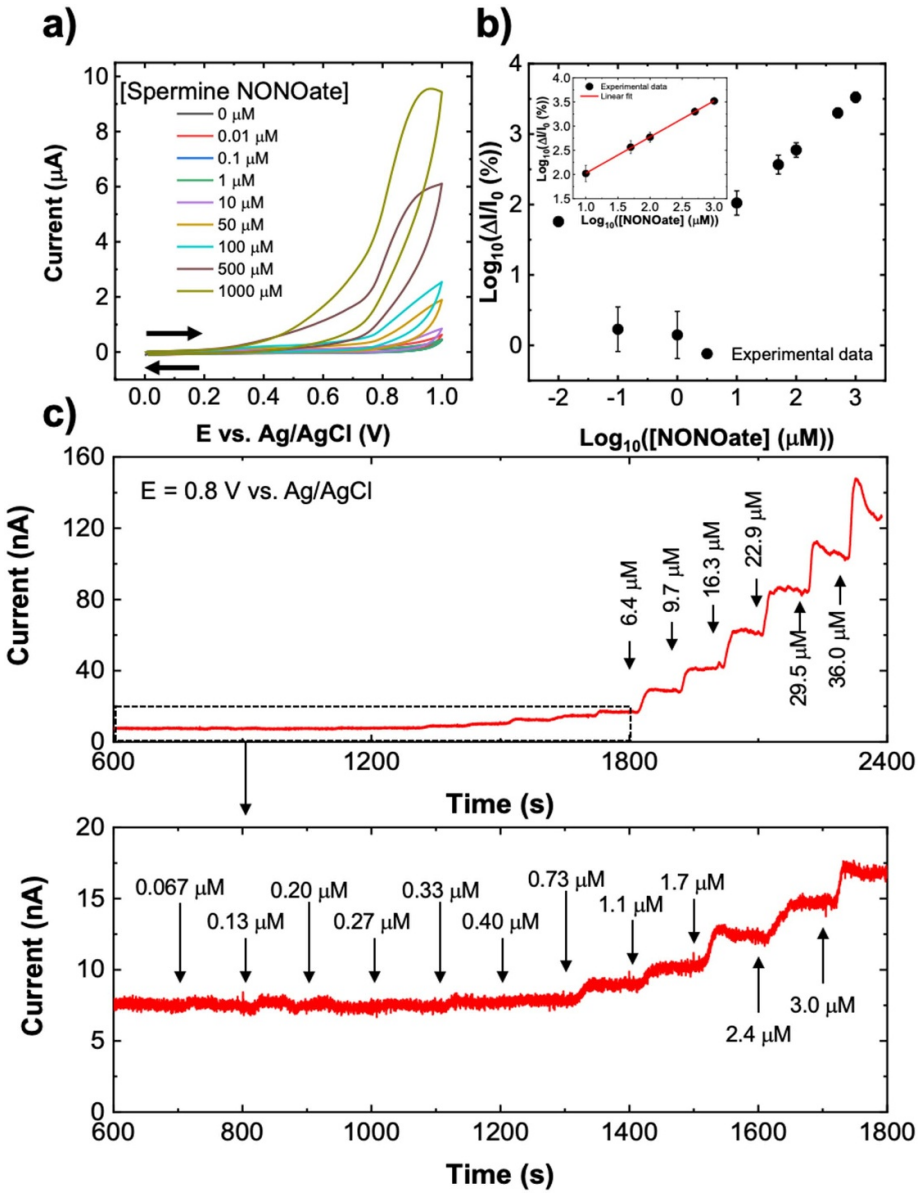

Figure 3. Electrochemical characterization with NO donor, spermine NONOate (SN). (a) Exemplary CV scans from 0 V to 1 V with increasing concentrations of SN (scan rate = 50 mV s^{-1}) and (b) the resulting calibration curve ($n = 4$). The inset highlights the dynamic range of our sensor along with the linear fit. (c) Chronoamperometric measurements ($E = 0.8$ V vs Ag/AgCl, stir rate = 400 rpm) across a range of SN concentrations with the bottom panel focusing on the low concentration region.

3.3. Morphological characterization of cells grown on fibronectin-modified graphene sensors

In vitro monitoring and detection of extracellular metabolites and byproducts is crucial for enabling high-throughput screening of therapeutics and a better understanding of various biophysical phenomena. To this end, we characterize the generation of NO in the MDA-MB-231 human breast cancer cell line, which can be stimulated with L-arginine to release NO (Marullo *et al* 2021). Cell attachment on graphene ink-coated substrates was monitored as a function of fibronectin concentration (10, 25, 50 μg ml^{-1}) used for coating the graphene surface. The number of attached cells per mm^2 of the substrate surface increases with increasing fibronectin concentration (SI figure S2). For electrochemical assays, graphene substrates were coated with 25 μg ml^{-1} fibronectin and cell morphologies were observed using phase contrast microscopy at 24 and 72 h post-seeding. While cells attach to the surfaces by 24 h post-seeding, the cells require more time to spread onto the surface (SI figure S3). Indeed, cells cultured on fibronectin-coated glass and graphene surfaces for 72 h exhibit increased spreading on the substrate surface as shown in microscopy images in figure 4(a) and as quantified in terms of a projected cell area in figure 4(b). Furthermore, the cells have an elongated morphology, which is characteristic of mesenchymal-like migratory cells, and is quantified by cell aspect ratio (figure 4(c)).

Table 1. Comparison of graphene-based electrochemical NO sensors.

Electrode material	NO source	Sensitivity	Detection limit	Peak potential	Cell tests	References
Graphene-hemin FET	DEA-NONOate in PBS	54 μS μM^{-1}	0.3 nM	N/A	RAW 264.7 w/ LPS, HUVECs w/bradykinin	(Jiang *et al* 2013)
PtW/rGO-IL	NO_2^- in PB (pH 2.5)	3.01 μA μM^{-1} cm^{-2}	0.13 nM	0.78 V vs. Ag/AgCl	None reported	(Govindhan and Chen 2016)
PtNPs-erGO	NO_2^- in PB (pH 2.5)	8.40 μA μM^{-1} cm^{-2}	52 nM	1.03 V vs. Ag/AgCl	None reported	(Mathew *et al* 2021)
AuPtNPs-rGO	NO saturated PBS (pH 7.2)	7.35 μA μM^{-1}	2.88 nM	0.724 V vs. Ag/AgCl	H9C2 w/L-arginine	(Liu *et al* 2016)
AuNPs-erGO	NO saturated PBS (pH 7.4)	5.38 μA μM^{-1} cm^{-2}	133 nM	0.821 V vs. Ag/AgCl	HUVECs w/acetylcholine	(Ting *et al* 2013)
Graphene/ RGD-peptide	N/A	N/A	25 nM	0.750 V vs. Ag/AgCl	HUVECs w/acetylcholine	(Guo *et al* 2012)
Graphene/ fibronectin	SN in PBS (pH 7.4)	0.748 (decade (%)) (decade [SN])$^{-1}$	10 μM SN	0.96 V vs. Ag/AgCl	MDA-MB-231 w/L-arginine	This work

FET = field-effect transistor, DEA = diethylamine, LPS = lipopolysaccharide, PB = phosphate buffer, PBS = phosphate buffered saline, NP = nanoparticle, IL = ionic liquid, rGO = reduced graphene oxide, erGO = electrochemically-reduced graphene oxide, RGD = Arginylglycylaspartic acid, SN = spermine NONOate.

To stimulate NO generation, L-arginine is added to the cells cultured on fibronectin-coated graphene, which promotes NO production enzymatically via NOS (Privett *et al* 2010). A previous study demonstrated that 4 mM L-arginine promotes an increase in NO generation in MCF7 breast cancer cells (Dou *et al* 2019). For our studies, 2 h after stimulation with 4 mM L-arginine, the cell morphology appears much more spherical, possibly due to the cells contracting in the presence of excess NO in the surrounding environment. Treatment with a NOS inhibitor can block L-arginine induced NO generation in MDA-MB-231 cells (Marullo *et al* 2021). To quench the NO generation, cells were treated with both L-arginine and L-NAME. After 2 h of stimulation, the inhibition of NO appears to promote a more well-attached and spread morphology. Figures 4(b) and (c) show the cell spread area and cell aspect ratio under different experimental conditions. Cells seeded on graphene and treated with L-arginine exhibited significantly lower cell spread areas and aspect ratios as compared to when cells were cultured on glass, graphene, and graphene with a combination of L-arginine and L-NAME treatments.

We also analyzed the viability of cells in response to treatment with L-arginine or a combination of L-arginine and L-NAME by performing a Live/Dead Assay. The presence of intracellular esterase activity in live cells converts calcein AM to calcein indicated by green fluorescence for live cells. On the other hand, ethidium homodimer-1 is absorbed by cells with a damaged cell membrane and it then binds to nucleic acid, producing a red fluorescence stain for dead cells. As shown in fluorescence microscopy images in figures 4(d), a large majority of cells treated with L-arginine or a combination of L-arginine and L-NAME for 2 h show green calcein staining and are thus viable. The percentage of live cells is higher than 90% for cells seeded on fibronectin-coated glass. Furthermore, approximately 80% of cells seeded on fibronectin-coated graphene substrates are viable both with and without treatment with the stimulants.

3.4. Electrochemical detection of extracellular NO with fibronectin-modified graphene sensors

After confirming successful attachment of cells to the fibronectin-modified graphene, amperometric measurements are carried out to detect extracellular NO from cells stimulated with L-arginine. A schematic of the test setup is shown in figure 5(a), in addition to an image of the test setup shown in figure S4 of the supplementary information. A PDMS well is attached to the sensor to house the cells and media during culturing. Before testing, the media is replaced with PBS to serve as the supporting electrolyte. Figure 5(b) shows the current-time profiles for four different experimental conditions (replicate experiments shown in supplementary figure S5). Like before, the cells are seeded on the sensor 72 h before testing to ensure there is enough time for cells to attach to the sensor surface. Allowing the cells to attach to the sensor surface helps minimize the cell-sensor distance, which is critical for detecting short-lived species, such as NO. All four experimental conditions show a sharp spike upon the addition of the L-arginine or L-arginine/L-NAME, which could be due to acute changes in the double-layer capacitance. For the cells with both L-arginine and L-NAME (red curve), the current quickly falls back to the baseline. However, for the cells with only L-arginine (grey curve), a broad dome-like feature and elevated current is seen after the initial

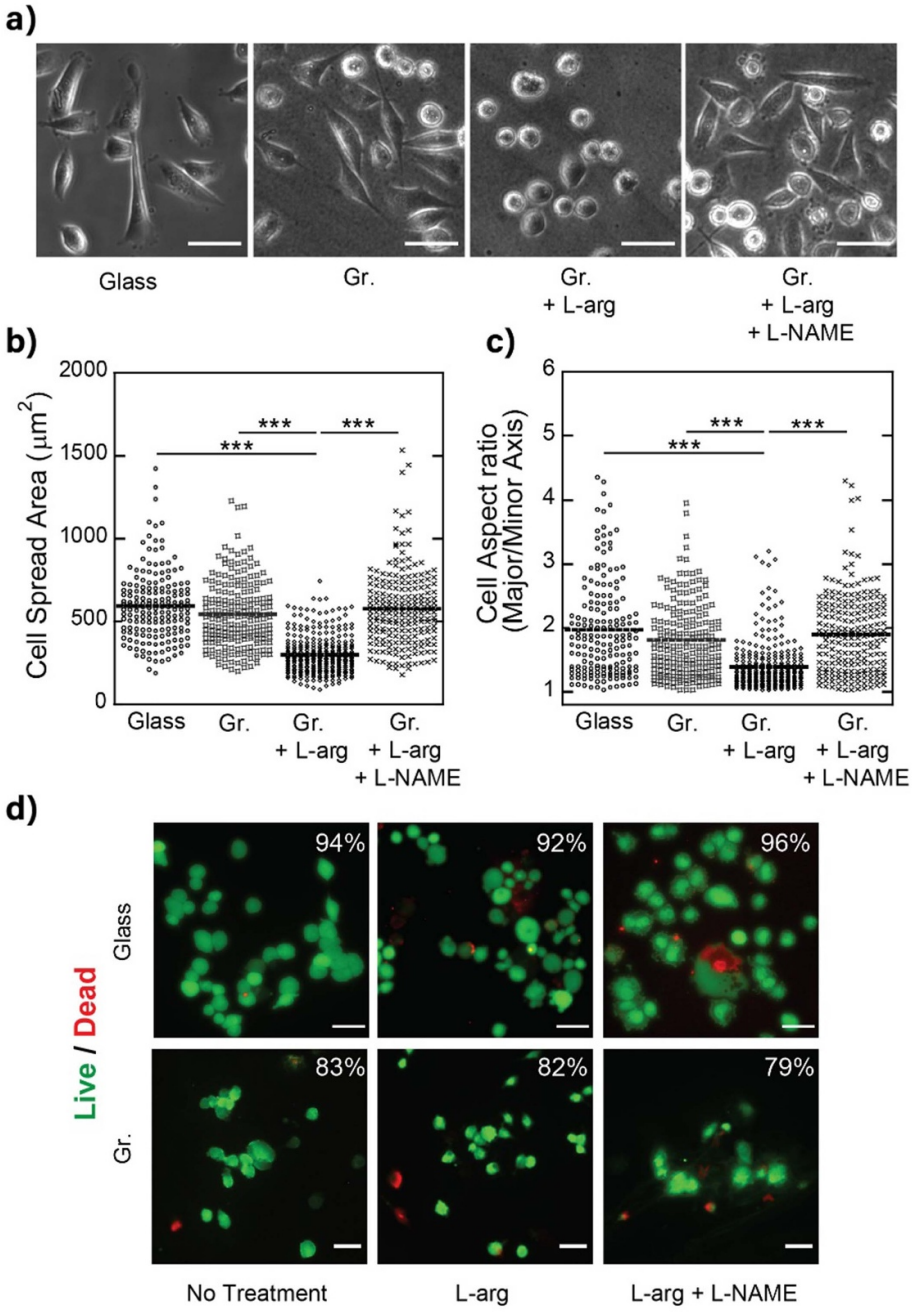

Figure 4. Characterization of cell attachment on graphene films coated with 25 μg ml^{-1} fibronectin. (a) Phase contrast microscopy images of MDA-MB-231 cells cultured for 72 h on glass, graphene, graphene after addition of 4 mM L-arginine, and after addition of 4 mM L-arginine and 8 mM L-NAME. Scale bars: 50 μm. Quantification of (b) cell spread area and (c) cell aspect ratio (elongation) for different treatment conditions. At least 170 cells were quantified for each treatment condition and the mean value is shown by the bold line. $^{***}p < 0.001$. (d) Fluorescence microscopy images from a Live (green)/Dead (red) assay for MDA-MB-231 cells seeded for 72 h on fibronectin-coated glass and graphene substrates then treated with L-arginine or L-arginine/L-NAME for 2 h. The percentage of viable cells for each treatment condition is indicated on the images. Scale bars: 50 μm.

spike. A similar feature has been observed in previous amperometric measurements with cells (Burmeister *et al* 2002, Walker *et al* 2007) and has been attributed to the release of multiple species with different kinetic behavior. While a similar feature is seen upon the addition of L-arginine in the absence of cells (blue curve), indicating the graphene electrode responds to L-arginine alone, the magnitude of the current increase is not as large as when cells are present. It is possible that the current increase seen after adding L-arginine to the cells contains contributions from both the L-arginine and the generated extracellular NO.

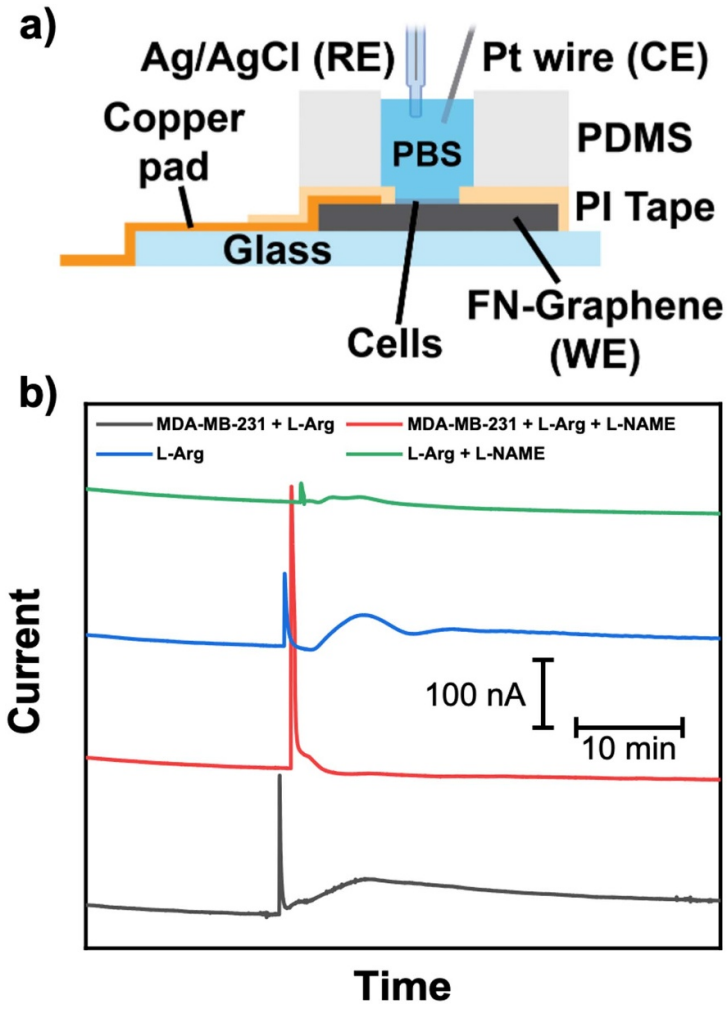

Figure 5. Real-time electrochemical monitoring of extracellular NO. (a) A schematic of the sensor with cells cultured directly on-chip. (b) Chronoamperometric measurements at $E = 0.8$ V vs. Ag/AgCl with cells (MDA-MB-231) stimulated by L-arginine (L-Arg) or a mixture of L-Arg and L-NAME.

4. Conclusion

This work demonstrates a solution-processed graphene ink film as a sensor for electrochemical detection of NO. By functionalizing the graphene film with a fibronectin extracellular matrix protein, human breast cancer cells are able to attach directly to the electrode surface, as confirmed by optical microscopy. Minimizing the cell-sensor spacing is important for NO detection due to its short lifetime in solution. With cells attached to the electrode surface, NO is detected in real-time using L-arginine to stimulate its generation. Profound changes in cell morphology are also observed upon adding L-arginine to the cell environment. We believe the acute elevation of NO levels in the surrounding environment has a deleterious effect on the cells and results in reduced spreading on the graphene surface. These effects are reversed after adding L-NAME, which quenches the generation of NO, further supporting this speculation.

Adapting this work to a future cardiovascular point-of-care device would require a number of changes and improvements. For instance, a point-of-care device that analyzes physiological samples would require improvements to sensor selectivity. This can be accomplished for example by coating the graphene with a NO-selective membrane (Thangavel and Ramaraj 2008, Shim *et al* 2010) or reducing the NO oxidation potential to minimize the contribution from interfering species, such as L-arginine. Moreover, a point-of-care device would require a more compact electrochemical cell, ideally with the reference, counter, and working electrodes all on-chip with a small footprint. While we did not demonstrate such a setup in this work, we have shown in a previous report an all-ink, on-chip electrochemical sensor for dopamine (Butler *et al* 2021). Furthermore, a point-of-care device based on the mechanism reported here would require specific handling and storage when being used in the field and maintaining the sterility/cleanliness of the sensor would also be critical.

Our target in this work was *ex vivo* application in order to study how cells respond to external

biochemical stimulation. *Ex vivo* cell experiments have great importance for drug development, disease modeling, and mechanistic characterization. Having the ability to monitor NO release in real-time, as opposed to periodically or using an endpoint assay, is crucial for these applications. NO levels can change quickly, and these dynamics may not be captured by periodic or endpoint measurements. However, even excessive NO levels for a short time can have adverse effects on cells and having the ability to detect the entirety of these fluctuations could provide better insight into underlying phenomena. Although this work focused on detecting NO, the demonstrated ability of these graphene films to support cell attachment makes them a potential platform to study other cell systems. For example, the affinity of graphene for dopamine could be useful for quantifying its concentrations in cultures of neural cells. Furthermore, the ease with which solution-processed graphene films can be deposited on various substrates, especially flexible and stretchable materials, could make them suitable for studying cells under mechanical stress.

Data availability statement

The data that support the findings of this study are available upon reasonable request from the authors.

Acknowledgments

The authors would like to acknowledge a Penn State College of Engineering Multidisciplinary Seed Grant. D B, P S K, and A E would like to acknowledge partial support from the NSF:I/UCRC Center for Atomically Thin Multifunctional Coatings (ATOMIC) (Division Of Engineering Education and Centers, Award No. 2113864), NSF Division of Electrical, Communications and Cyber Systems (ECCS, Award No. 2236997), and the National Institutes of Health (Award No. R21EB031354). The content of this report is solely the responsibility of the authors and does not necessarily represent the official views of the National Science Foundation (NSF) or National Institutes of Health (NIH). C S was supported in part by Penn State Leighton Riess Graduate Fellowship in Engineering. The authors are also grateful for the staff and resources of the Materials Characterization Lab at the Penn State Materials Research Institute.

Conflict of interest

The authors have no conflicts of interest to declare.

ORCID iD

Derrick Butler https://orcid.org/0000-0003-3514-9326

References

Bard A J, Faulkner L R and White H S 2022 *Electrochemical Methods: Fundamentals and Applications* 3rd edn (Wiley)

Bolotsky A, Butler D, Dong C, Gerace K, Glavin N R, Muratore C, Robinson J A and Ebrahimi A 2019 Two-dimensional materials in biosensing and healthcare: from in vitro diagnostics to optogenetics and beyond *ACS Nano* **13** 9781–810

Burmeister J J, Pomerleau F, Palmer M, Day B K, Huettl P and Gerhardt G A 2002 Improved ceramic-based multisite microelectrode for rapid measurements of l-glutamate in the CNS *J. Neurosci. Methods* **119** 163–71

Butler D, Moore D, Glavin N R, Robinson J A and Ebrahimi A 2021 Facile post-deposition annealing of graphene ink enables ultrasensitive electrochemical detection of dopamine *ACS Appl. Mater. Interfaces* **13** 11185–94

Cançado L G, Jorio A, Ferreira E H M, Stavale F, Achete C A, Capaz R B, Moutinho M V O, Lombardo A, Kulmala T S and Ferrari A C 2011 Quantifying defects in graphene via Raman spectroscopy at different excitation energies *Nano Lett.* **11** 3190–6

Chen H and Zhao G 2012 Nanocomposite of polymerized ionic liquid and graphene used as modifier for direct electrochemistry of cytochrome c and nitric oxide biosensing *J. Solid State Electrochem.* **16** 3289–97

Chung A W *et al* 2021 A phase 1/2 clinical trial of the nitric oxide synthase inhibitor L-NMMA and taxane for treating chemoresistant triple-negative breast cancer *Sci. Transl. Med.* **13** eabj5070

Conner E M and Grisham M B 1995 Nitric oxide: biochemistry, physiology, and pathophysiology *Methods* **7** 3–13

Córdoba-Torres P, Mesquita T J and Nogueira R P 2015 Relationship between the origin of constant-phase element behavior in electrochemical impedance spectroscopy and electrode surface structure *J. Phys. Chem.* C **119** 4136–47

Derojas-Walker T, Tamny S, Ji H, Wishnok J S and Tannenbaum S R 1995 Nitric oxide induces oxidative damage in addition to deamination in macrophage DNA *Chem. Res. Toxicol.* **8** 473–7

Dou B, Li J, Jiang B, Yuan R and Xiang Y 2019 DNAlated *in situ* synthesis of highly dispersed AuNPs on nitrogen-doped graphene for real-time electrochemical monitoring of nitric oxide released from live cancer cells *Anal. Chem.* **91** 2273–8

Džoljić E, Grbatinić I and Kostić V 2015 Why is nitric oxide important for our brain? *Funct. Neurol.* **30** 159–63

Ferrari A C and Robertson J 2004 Raman spectroscopy of amorphous, nanostructured, diamond-like carbon, and nanodiamond *Phil. Trans. R. Soc.* A **362** 2477–512

Frahs S M *et al* 2019 Prechondrogenic ATDC5 cell attachment and differentiation on graphene foam; modulation by surface functionalization with fibronectin *ACS Appl. Mater. Interfaces* **11** 41906–24

Garbán H J and Bonavida B 1999 Nitric oxide sensitizes ovarian tumor cells to fas-induced apoptosis *Gynecol. Oncol.* **73** 257–64

Geetha Bai R, Muthoosamy K, Zhou M, Ashokkumar M, Huang N M and Manickam S 2017 Sonochemical and sustainable synthesis of graphene-gold (G-Au) nanocomposites for enzymeless and selective electrochemical detection of nitric oxide *Biosens. Bioelectron.* **87** 622–9

Govindhan M and Chen A 2016 Enhanced electrochemical sensing of nitric oxide using a nanocomposite consisting of platinum-tungsten nanoparticles, reduced graphene oxide and an ionic liquid *Microchim. Acta* **183** 2879–87

Guo C X, Ng S R, Khoo S Y, Zheng X, Chen P and Li C M 2012 RGD-peptide functionalized graphene biomimetic live-cell sensor for real-time detection of nitric oxide molecules *ACS Nano* **6** 6944–51

Guo J, Wei T, Huang Q, Li M, Yang C, Mou J, Shi L, Gao T and Li G 2022 Direct acupuncture of nitric oxide by an

electrochemical microsensor with high time-space resolution *Biosens. Bioelectron.* **195** 113667
Habib S and Ali A 2011 Biochemistry of nitric oxide *Indian J. Clin. Biochem.* **26** 3–17
Hall C N and Garthwaite J 2009 What is the real physiological NO concentration in vivo? *Nitric Oxide-Biol. Chem.* **2** 92–103
He G W and Liu Z G 2001 Comparison of nitric oxide release and endothelium-derived hyperpolarizing factor-mediated hyperpolarization between human radial and internal mammary arteries *Circulation* **104** 344–9
Heales S J R, Bolaños J P, Stewart V C, Brookes P S, Land J M and Clark J B 1999 Nitric oxide, mitochondria and neurological disease *Biochim. Biophys. Acta* **1410** 215–28
Heinecke J L *et al* 2014 Tumor microenvironment-based feed-forward regulation of NOS2 in breast cancer progression *Proc. Natl Acad. Sci. USA* **111** 6323–8
Jiang S, Cheng R, Wang X, Xue T, Liu Y, Nel A, Huang Y and Duan X 2013 Real-time electrical detection of nitric oxide in biological systems with sub-nanomolar sensitivity *Nat. Commun.* **4** 1–7
Kenry, Chaudhuri P K, Loh K P and Lim C T 2016 Selective accelerated proliferation of malignant breast cancer cells on planar graphene oxide films *ACS Nano* **10** 3424–34
Korde Choudhari S, Chaudhary M, Bagde S, Gadbail A R and Joshi V 2013 Nitric oxide and cancer: a review *World J. Surg. Oncol.* **11** 1–11
Kovtun A, Jones D, Dell'Elce S, Treossi E, Liscio A and Palermo V 2019 Accurate chemical analysis of oxygenated graphene-based materials using x-ray photoelectron spectroscopy *Carbon* **143** 268–75
Leiro J A, Heinonen M H, Laiho T and Batirev I G 2003 Core-level XPS spectra of fullerene, highly oriented pyrolitic graphite, and glassy carbon *J. Electron Spectros. Relat. Phenom.* **128** 205–13
Li J, Xie J, Gao L and Li C M 2015 Au nanoparticles-3D graphene hydrogel nanocomposite to boost synergistically *in situ* detection sensitivity toward cell-released nitric oxide *ACS Appl. Mater. Interfaces* **7** 2726–34
Lim M H, Xu D and Lippard S J 2006 Visualization of nitric oxide in living cells by a copper-based fluorescent probe *Nat. Chem. Biol.* **2** 375–80
Liu H, Duan C, Yang C, Shen W, Wang F and Zhu Z 2015 A novel nitrite biosensor based on the direct electrochemistry of hemoglobin immobilized on MXene-Ti_3C_2 *Sens. Actuators* B **218** 60–66
Liu Y M, Punckt C, Pope M A, Gelperin A and Aksay I A 2013 Electrochemical sensing of nitric oxide with functionalized graphene electrodes *ACS Appl. Mater. Interfaces* **5** 12624–30
Liu Z, Forsyth H, Khaper N and Chen A 2016 Sensitive electrochemical detection of nitric oxide based on AuPt and reduced graphene oxide nanocomposites *Analyst* **141** 4074–83
Liu Z, Nemec-Bakk A, Khaper N and Chen A 2017 Sensitive electrochemical detection of nitric oxide release from cardiac and cancer cells via a hierarchical nanoporous gold microelectrode *Anal. Chem.* **89** 8036–43
Loibl S, Von Minckwitz G, Weber S, Sinn H P, Schini-Kerth V B, Lobysheva I, Nepveu F, Wolf G, Strebhardt K and Kaufmann M 2002 Expression of endothelial and inducible nitric oxide synthase in benign and malignant lesions of the breast and measurement of nitric oxide using electron paramagnetic resonance spectroscopy *Cancer* **95** 1191–8
Macmicking J, Xie Q-W and Nathan C N 1997 Nitric oxide and macrophage function *Annu. Rev. Immunol.* **15** 350
Maiorana A, O'Driscoll G, Taylor R and Green D 2012 Exercise and the nitric oxide vasodilator system *Sports Med.* **33** 1013–35
Maity G, Choudhury P R, Sen T, Ganguly K K, Sil H and Chatterjee A 2011 Culture of human breast cancer cell line (MDA-MB-231) on fibronectin-coated surface induces pro-matrix metalloproteinase-9 expression and activity *Tumor Biol.* **32** 129–38
Majumder S *et al* 2014 A comparative study of NONOate based NO donors: spermine NONOate is the best suited NO donor for angiogenesis *Nitric Oxide-Biol. Chem.* **36** 76–86
Marullo R *et al* 2021 The metabolic adaptation evoked by arginine enhances the effect of radiation in brain metastases *Sci. Adv.* **7** eabg1964
Mathew G, Narayanan N, Abraham D A, De M and Neppolian B 2021 Facile green approach for developing electrochemically reduced graphene oxide-embedded platinum nanoparticles for ultrasensitive detection of nitric oxide *ACS Omega* **6** 8068–80
Michel T and Feron O 1997 Perspective series: nitric oxide and nitric oxide synthases nitric oxide synthases: which, where, how, and why? *J. Clin. Invest.* **100** 2146–52
Mocellin S, Bronte V and Nitti D 2007 Nitric oxide, a double edged sword in cancer biology: searching for therapeutic opportunities *Med. Res. Rev.* **27** 317–52
Nagano T 1999 Practical methods for detection of nitric oxide *Luminescence* **14** 283–90
Nguyen E P, Silva C D C C and Merkoçi A 2020 Recent advancement in biomedical applications on the surface of two-dimensional materials: from biosensing to tissue engineering *Nanoscale* **12** 19043–67
Pinder A G, Rogers S C, Khalatbari A, Ingram T E and James P E 2008 The measurement of nitric oxide and its metabolites in biological samples by ozone-based chemiluminescence *Methods Mol. Biol.* **476** 11–28
Privett B J, Shin J H and Schoenfisch M H 2010 Electrochemical nitric oxide sensors for physiological measurements *Chem. Soc. Rev.* **39** 1925–35
Quinton D, Girard A, Thi Kim L T, Raimbault V, Griscom L, Razan F, Griveau S and Bedioui F 2011 On-chip multi-electrochemical sensor array platform for simultaneous screening of nitric oxide and peroxynitrite *Lab Chip* **11** 1342
Ramamurthi A and Lewis R S 1997 Measurement and modeling of nitric oxide release rates for nitric oxide donors *Chem. Res. Toxicol.* **10** 408–13
Reveneau S, Arnould L, Jolimoy G, Hilpert S, Lejeune P, Saint-Giorgio V, Belichard C and Jeannin J F 1999 Nitric oxide synthase in human breast cancer is associated with tumor grade, proliferation rate, and expression of progesterone receptors *Lab. Invest.* **79** 1215–25
Rohaizad N, Mayorga-Martinez C C, Fojtů M, Latiff N M and Pumera M 2021 Two-dimensional materials in biomedical, biosensing and sensing applications *Chem. Soc. Rev.* **50** 619–57
Secor E B, Ahn B Y, Gao T Z, Lewis J A and Hersam M C 2015 Rapid and versatile photonic annealing of graphene inks for flexible printed electronics *Adv. Mater.* **27** 6683–8
Shahid M M, Rameshkumar P, Pandikumar A, Lim H N, Ng Y H and Huang N M 2015 An electrochemical sensing platform based on a reduced graphene oxide–cobalt oxide nanocube@platinum nanocomposite for nitric oxide detection *J. Mater. Chem.* A **3** 14458–68
Shim J H, Do H and Lee Y 2010 Simple fabrication of amperometric nitric oxide microsensors based on electropolymerized membrane films *Electroanalysis* **22** 359–66
Sun J, Zhang X, Broderick M and Fein H 2003 Measurement of nitric oxide production in biological systems by using griess reaction assay *Sensors* **3** 276–84
Suvarnaphaet P and Pechprasarn S 2017 Graphene-based materials for biosensors: a review *Sensors* **17** 2161
Taherian A, Li X, Liu Y and Haas T A 2011 Differences in integrin expression and signaling within human breast cancer cells *BMC Cancer* **11** 293
Thangavel S and Ramaraj R 2008 Polymer membrane stabilized gold nanostructures modified electrode and its application in nitric oxide detection *J. Phys. Chem.* C **112** 19825–30
Thi Kim L T O, Escriou V, Griveau S, Girard A, Griscom L, Razan F and Bedioui F 2014 Array of ultramicroelectrodes

for the simultaneous detection of nitric oxide and peroxynitrite in biological systems *Electrochim. Acta* **140** 33–36

Thomas D D, Liu X, Kantrow S P and Lancaster J R 2001 The biological lifetime of nitric oxide: implications for the perivascular dynamics of NO and O_2 *Proc. Natl Acad. Sci. USA* **98** 355–60

Ting S L, Guo C X, Leong K C, Kim D H, Li C M and Chen P 2013 Gold nanoparticles decorated reduced graphene oxide for detecting the presence and cellular release of nitric oxide *Electrochim. Acta* **111** 441–6

Tolba M, Ahmed M U, Tlili C, Eichenseher F, Loessner M J and Zourob M 2012 A bacteriophage endolysin-based electrochemical impedance biosensor for the rapid detection of Listeria cells *Analyst* **137** 5749–56

Vakkala M, Kahlos K, Lakari E, Pääkkö P, Kinnula V, Soini Y and Medicine I 2000 Inducible nitric oxide synthase expression, apoptosis, and angiogenesis in *in situ* and invasive breast carcinomas *Clin. Cancer Res.* **6** 2408–16

Walker E, Wang J, Hamdi N, Monbouquette H G and Maidment N T 2007 Selective detection of extracellular glutamate in brain tissue using microelectrode arrays coated with over-oxidized poly pyrrole *Analyst* **132** 1107–11

Walsh E M, Keane M M, Wink D A, Callagy G and Glynn S A 2016 Review of triple negative breast cancer and the impact of inducible nitric oxide synthase on tumor biology and patient outcomes *Crit. Rev. Oncog.* **21** 333–51

Wang M, Zhu L, Zhang S, Lou Y, Zhao S, Tan Q, He L and Du M 2021 A copper(II) phthalocyanine-based metallo-covalent organic framework decorated with silver nanoparticle for sensitively detecting nitric oxide released from cancer cells *Sens. Actuators* B **338** 129826

Weaver J, Porasuphatana S, Tsai P, Budzichowski T and Rosen G M 2005 Spin trapping nitric oxide from neuronal nitric oxide synthase: a look at several iron-dithiocarbamate complexes *Free Radic. Res.* **39** 1027–33

Wu J F, Xu M Q and Zhao G C 2010 Graphene-based modified electrode for the direct electron transfer of Cytochrome c and biosensing *Electrochem. Commun.* **12** 175–7

Xu T, Scafa N, Xu L P, Su L, Li C, Zhou S, Liu Y and Zhang X 2014 Electrochemical sensors for nitric oxide detection in biological applications *Electroanalysis* **26** 449–68

Xu W, Liu L Z, Loizidou M, Ahmed M and Charles I G 2002 The role of nitric oxide in cancer *Cell Res.* **12** 311–20

Yoon J, Shin J-W, Lim J, Mohammadniaei M, Bharate Bapurao G, Lee T and Choi J-W 2017 Electrochemical nitric oxide biosensor based on amine-modified MoS_2/graphene oxide/myoglobin hybrid *Colloids Surf.* B **159** 729–36

Zhang J and Oyama M 2005 Gold nanoparticle arrays directly grown on nanostructured indium tin oxide electrodes: characterization and electroanalytical application *Anal. Chim. Acta* **540** 299–306

Zhong J H, Zhang J, Jin X, Liu J Y, Li Q, Li M H, Cai W, Wu D Y, Zhan D and Ren B 2014 Quantitative correlation between defect density and heterogeneous electron transfer rate of single layer graphene *J. Am. Chem. Soc.* **136** 16609–17